PNAS RESEARCH ARTICLE | NEUROSCIENCE

Insulin regulates neurovascular coupling through astrocytes

Ana M. Fernandez[a,b], Laura Martinez-Rachadell[a,b], Marta Navarrete[a], Julia Pose-Utrilla[b,c], Jose Carlos Davila[b,d], Jaime Pignatelli[a,b], Sonia Diaz-Pacheco[a], Santiago Guerra-Cantera[a,b], Emilia Viedma-Moreno[a,b], Rocio Palenzuela[e], Samuel Ruiz de Martin Esteban[e], Ricardo Mostany[f], Cristina Garcia-Caceres[g], Matthias Tschöp[g], Teresa Iglesias[b,c], Maria L. de Ceballos[a], Antonia Gutierrez[b,d], and Ignacio Torres Aleman[b,h,i,1]

Edited by C. Ronald Kahn, Harvard Medical School, Boston, MA; received March 16, 2022; accepted May 10, 2022

Mice with insulin receptor (IR)–deficient astrocytes (GFAP-IR knockout [KO] mice) show blunted responses to insulin and reduced brain glucose uptake, whereas IR-deficient astrocytes show disturbed mitochondrial responses to glucose. While exploring the functional impact of disturbed mitochondrial function in astrocytes, we observed that GFAP-IR KO mice show uncoupling of brain blood flow with glucose uptake. Since IR-deficient astrocytes show higher levels of reactive oxidant species (ROS), this leads to stimulation of hypoxia-inducible factor-1α and, consequently, of the vascular endothelial growth factor angiogenic pathway. Indeed, GFAP-IR KO mice show disturbed brain vascularity and blood flow that is normalized by treatment with the antioxidant *N*-acetylcysteine (NAC). NAC ameliorated high ROS levels, normalized angiogenic signaling and mitochondrial function in IR-deficient astrocytes, and normalized neurovascular coupling in GFAP-IR KO mice. Our results indicate that by modulating glucose uptake and angiogenesis, insulin receptors in astrocytes participate in neurovascular coupling.

insulin | astrocytes | neurovascular coupling

Significance

Disturbed insulin actions in the brain have been related to various brain diseases, making the study of brain actions of this hormone a topic of great interest. We find that through its receptors in astrocytes, insulin controls coupling of brain glucose uptake with blood flow, which is key to support brain activity in response to functional demands. Under conditions of insufficient insulin input onto astrocytes, development of excess oxidative stress, which is associated with different brain conditions and is amenable to therapeutic amelioration, appears to interfere with this function of insulin.

The pancreatic hormone insulin is not only a major regulator of body energy handling, but also exerts many other functions, including vasoactive effects (1, 2) that may modulate brain perfusion (3). Indeed, endothelial dysfunction is associated with insulin resistance (4) and is reflected in reduced cerebral perfusion (5), leading to suboptimal oxygen levels in the brain. In this organ, astrocytes sense changes in oxygen pressure (PO_2), providing feedback information to processes involved in cerebral perfusion (6) through a mechanism under intense scrutiny (7). In this way, astrocytes, together with other cellular components of the neurovascular unit, are involved in neurovascular responses to changes in brain activity (8). Because brain metabolic demands and blood flow are coupled through functional hyperemia (9), astrocytes, that are sensitive to insulin, have been proposed to participate both in glucose and O_2 sensing (7).

We recently showed that insulin receptors in astrocytes participate in brain glucose handling and the responses of these cells to glucose (10). In turn, astrocytes have an intricate relationship with brain vessels through their end feet (11), placing them at the crossroad between metabolic and vasoactive signals. Indeed, PO_2 modulates vessel formation in conjunction with metabolism (12). Ultimately, the size of the brain vascular tree will affect the level of perfusion to this organ. Because changes in brain perfusion and metabolism are associated with aging (13), are exacerbated in parallel in different brain pathologies (8), and probably herald development of Alzheimer's disease (AD) (14), we examined the role of astrocytic insulin receptors (IRs) in brain perfusion, as insulin resistance is associated with aging and neurodegeneration.

Ablation of IRs in astrocytes blocked entrance of, and brain responses to, circulating insulin, suggesting that astrocytes form part of the intercellular pathway of passage of this hormone into the brain. In vivo and in vitro analysis of the role of astrocytic IRs in brain function revealed that glucose uptake and brain perfusion are integrated by astrocytic IRs. This receptor is essential to maintain normal astrocytic mitochondrial function and brain vascularization. Therefore, insulin modulates brain physiology through astrocytes beyond central regulation of glucose allocation.

Results

Brain Activation by Circulating Insulin Involves IRs in Glial End Feet. We first determined whether IRs are present in astrocytic end feet ensheathing endothelial cells of the blood–brain barrier (BBB), as its presence in this compartment may allow circulating insulin to be taken up by astrocytes. Using combined IR immunogold labeling and electron microscopy we localized these receptors in astrocytic end feet (Fig. 1*A* and *B*,

Author contributions: A.M.F., M.N., T.I., A.G., and I.T.A. designed research; A.M.F., L.M.-R., M.N., J.P.-U., J.C.D., J.P., S.D.-P., S.G.-C., E.V.-M., and M.L.d.C. performed research; R.P., S.R.d.M.E., R.M., C.G.-C., and M.T. contributed new reagents/analytic tools; A.M.F., L.M.-R., M.N., J.P.-U., J.C.D., J.P., S.D.-P., T.I., M.L.d.C., A.G., and I.T.A. analyzed data; and A.M.F. and I.T.A. wrote the paper.

The authors declare no competing interest.

This article is a PNAS Direct Submission.

[1]To whom correspondence may be addressed. Email: ignacio.torres@achucarro.org.

This article contains supporting information online at http://www.pnas.org/lookup/suppl/doi:10.1073/pnas.2204527119/-/DCSupplemental.

Published July 14, 2022.

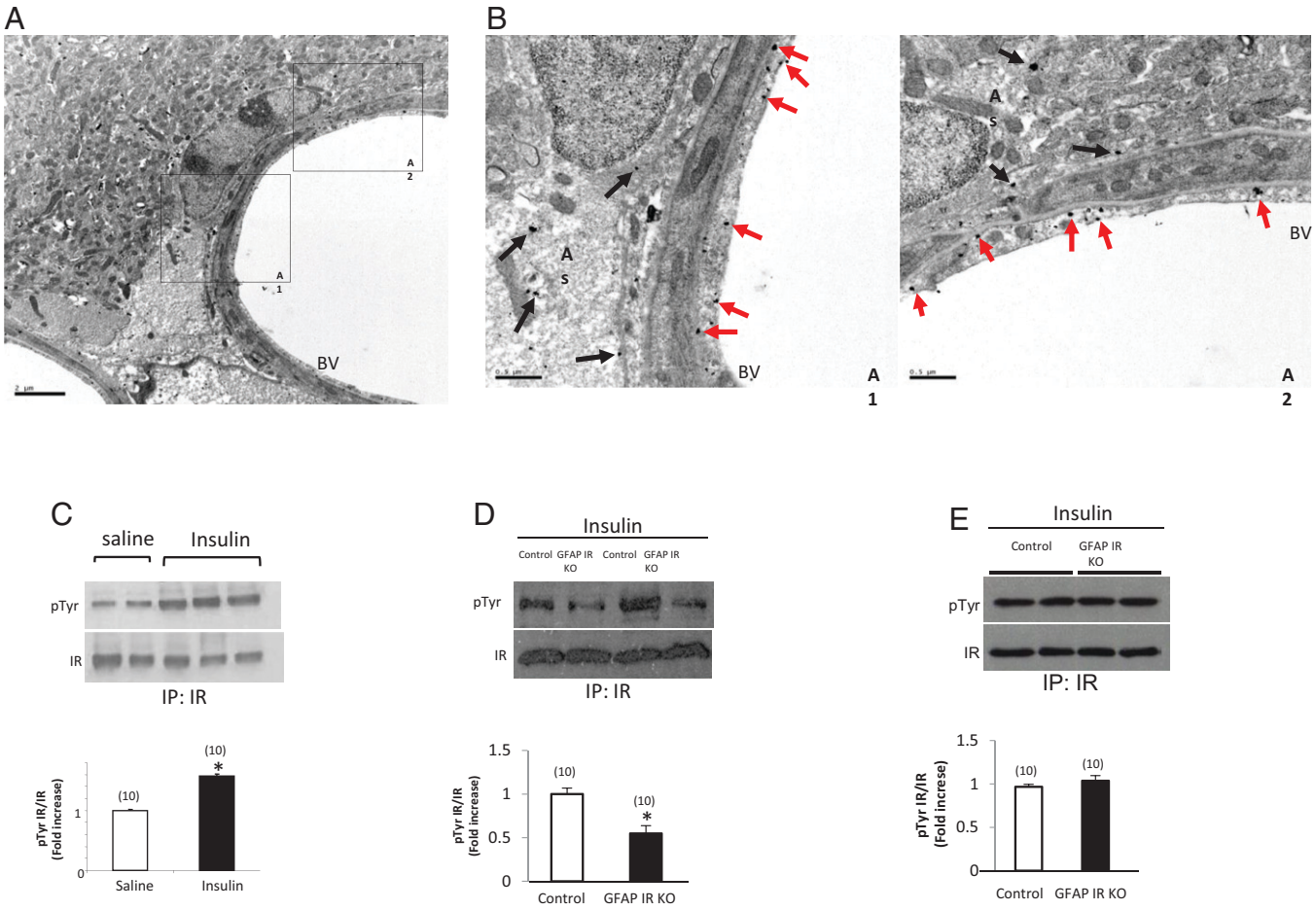

Fig. 1. IRs in astrocyte end feet are needed for brain IR activation by peripheral insulin. (*A*) Electron microscopy photograph using immunogold labeling for IRs, illustrating the presence of immunoreactive IR deposits in astroglial end feet surrounding brain capillaries and in endothelial cells. (*B*) A1 and A2 squares from *A*, are shown at greater magnification. Note the presence of IR gold particles in endothelial cells (red arrows) and astrocytic end feet (black arrows). (Scale bar in *A*, 2 μm and in *B*, 0.5 μm.) BV, brain vessel. (*C*) Phosphorylation of IRs in mouse somatosensory cortex after intraperitoneal injection of insulin (3 IU/kg body weight) or saline ($n = 10$; t test, t = 3.54, $^*P < 0.05$). (*D*) Phosphorylation of IRs after intraperitoneal injection of insulin in somatosensory cortex of GFAP-IR KO mice and littermates injected with corn oil ($n = 10$; t test, t = 3.27, $^*P < 0.05$, $n = 10$). (*E*) Phosphorylation of IRs in skeletal muscle of GFAP-IR KO mice and littermates after intraperitoneal injection of insulin (3 IU/kg body weight). Activation of IRs is shown as amount of tyrosine phosphorylated receptor (pTyr) normalized by total levels of immunoprecipitated IR ($n = 10$). Representative blots are shown.

black arrows). This anatomical location, in close proximity to endothelial cells that also express the IR (Fig. 1*B*, red arrows), may allow the passage of circulating insulin into astrocytes by transcytosis through endothelial cells (15).

As already documented (16), systemic administration of insulin results in significant activation of brain IRs ($^*P < 0.05$ vs. saline, t test; Fig. 1*C*). However, GFAP-IR knockout (KO) mice show attenuated responses to peripheral insulin injection (3 IU/kg, 100 μL), as determined by significantly reduced phosphorylation of brain ($^*P < 0.05$ vs. littermate controls, t test; Fig. 1*D*), but not muscle IRs (Fig. 1*E*). The reduction in brain IR phosphorylation was not related to lower brain IR levels in mutant mice due to the ablation of astrocytic IRs ($^{**}P < 0.01$ vs. control littermates, t test; *SI Appendix*, Fig. S1*A* and S1), since receptor activation was normalized to relative levels (similar between tamoxifen-treated and nontreated mice; see *Lower* blot in Fig. 1*D*). Conversely, direct intraparenchymal insulin injection (3 IU/2 μL) into the brain of GFAP-IR KO mice resulted in IR activation similar to littermate controls (*SI Appendix*, Fig. S1*B*). Furthermore, GFAP-IR KO mice show normal brain insulin-like growth factor I (IGF-I) receptor phosphorylation in response to systemic injection (1 μg/g intraperitoneally [i.p.]) of this close relative of insulin (*SI Appendix*, Fig. S1*C*), indicating specific loss of brain sensitivity to systemic insulin. In addition, control $IR^{f/f}$ mice injected with tamoxifen show preserved brain IR phosphorylation in response to systemic insulin (*SI Appendix*, Fig. S1*D*).

Since changes in intracellular Ca^{2+} levels are used as a proxy of astrocyte activity (17), we determined whether circulating insulin modulates intracellular Ca^{2+} in astrocytes of GFAP-IR KO mice. We monitored in vivo Ca^{2+} levels in astrocytes located in the somatosensory cortex by two-photon laser-scanning fluorescence microscopy using a genetically encoded Ca^{2+} indicator (Lck-GCaMP6f) (Fig. 2*A* and *B*). We found that systemic administration of insulin (3 IU/kg; 100 μL), elicited increases in Ca^{2+} spike frequency in control littermates but not in GFAP-IR KO mice ($^{**}P < 0.01$, Kruskal–Wallis followed by a Wilcoxon test; Fig. 2*C* and *D*), confirming that astrocytes directly respond to systemic insulin and that the IR is mediating this effect.

To trace cellular pathways involved in the passage of blood-borne insulin into the brain, we injected mice with digoxigenin-labeled insulin (Dig-Ins, 3 μg/100 μL; *SI Appendix*, Fig. S2*A*) in the carotid artery and examined its route of entrance by double immunolabeling with anti-Dig and cell-specific markers after careful transcardial saline perfusion (*Materials and Methods*). In GFAP-IR KO mice injected with vehicle (oil), digoxigenin staining was readily seen in cell somas of neuronal appearance and in the parenchyma (Fig. 3*A*, *b* and *c*). Double immunostaining

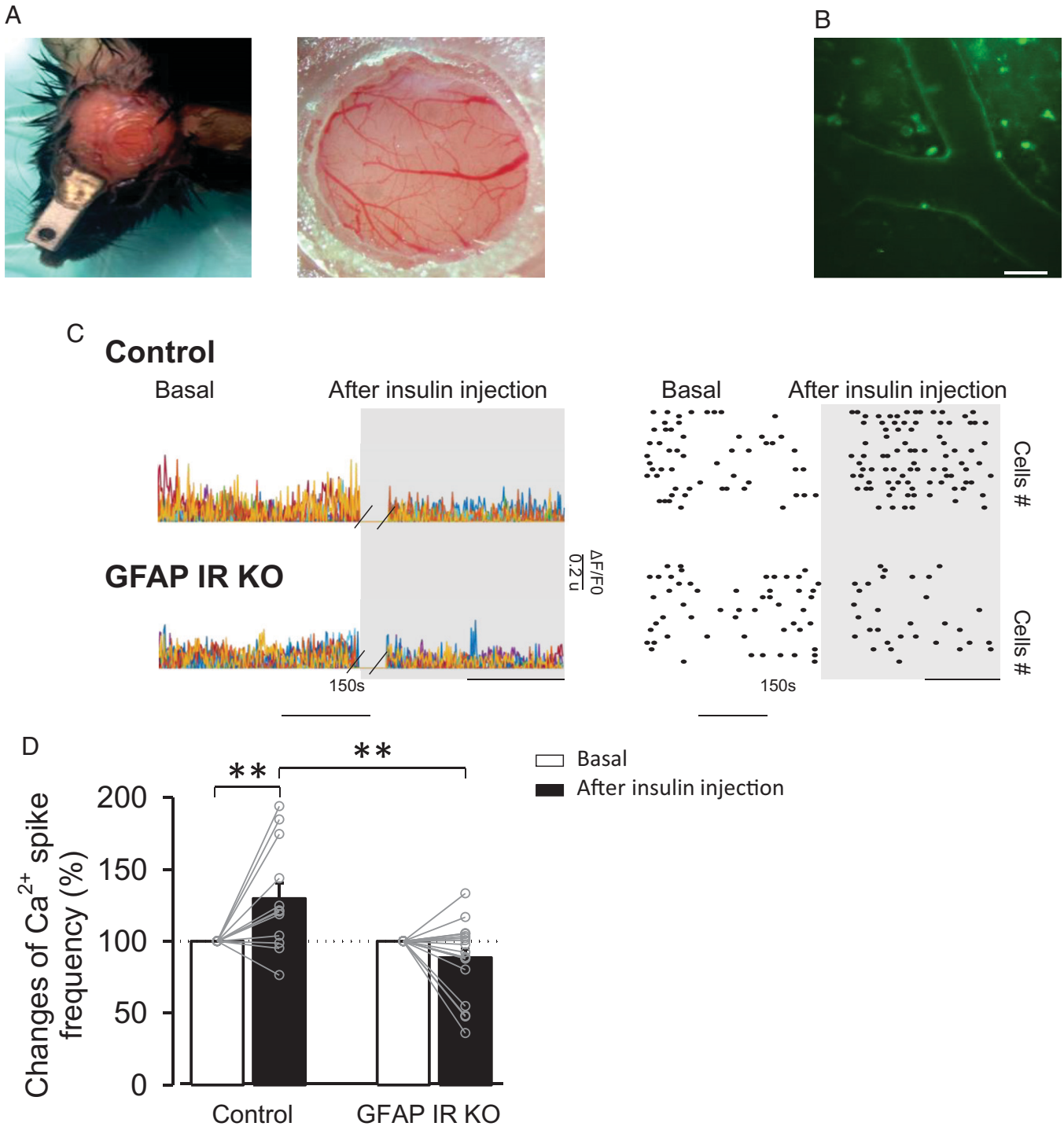

Fig. 2. Peripheral insulin modulates astrocyte activity. (*A*) Mouse bearing a cranial window (*Left*) and a macroscopic image of the mouse cranial window (*Right*). (*B*) Representative two-photon fluorescence intensities for viral transfection of AAV5-P_{GFAP}-Lck-GCaMP6f in somatosensory cortex imaging in vivo. Note astrocytic end feet enwrapping blood vessels. (Scale bar, 35 μm.) (*C*, *Left*) Representative experiments showing the amplitude of calcium events vs. time 5 min before (basal) and 15 min after i.p. injection of insulin (3 IU/kg body weight) in control littermates (*Top*) and GFAP-IR KO (*Bottom*) mice. (*Right*) Representative raster plot of ROI activity vs. time showing the frequency of calcium events 5 min before (basal) and 15 min after injection of insulin in control (*Top*) and GFAP-IR KO (*Bottom*) mice. (*D*) Changes of spike frequency of Ca^{2+} signals per area 5 min before (basal) and 15 min after i.p. injection of insulin in control ($n = 12$ from $n = 4$ mice, $P < 0.01$ Wilcoxon test) and GFAP-IR KO ($n = 19$ from $n = 4$ mice, $P = 0.163$ Wilcoxon test) mice. Differences between groups were determined by Kruskal–Wallis test (**$P < 0.01$).

with anti-Dig and anti-NeuN, a neuronal marker, confirmed that neurons accumulate Dig after peripheral injection of Dig-Ins, in an IR-dependent manner (Fig. 3*B* and *D*). However, in tamoxifen-treated GFAP-IR KO mice, Dig staining was much less intense in the parenchyma, and neuronal-like somas were absent (Fig. 3*C*, *b* and *c*, and *D*). In addition, Dig-Ins staining in vessels was seen only in GFAP-IR KO mice (Fig. 3*C*, *a*, and *SI Appendix*, Fig. S2*B*). Quantification of double-stained Dig^+/$NeuN^+$ cells confirmed that GFAP-IR KO mice accumulate very little amount of Dig, as compared to controls. Since all animals were profusely perfused with saline before immunocytochemistry was performed, this suggests that in the absence of astrocytic IRs, Dig-Ins is retained in the endothelium without crossing into the brain parenchyma. As already reported (10),

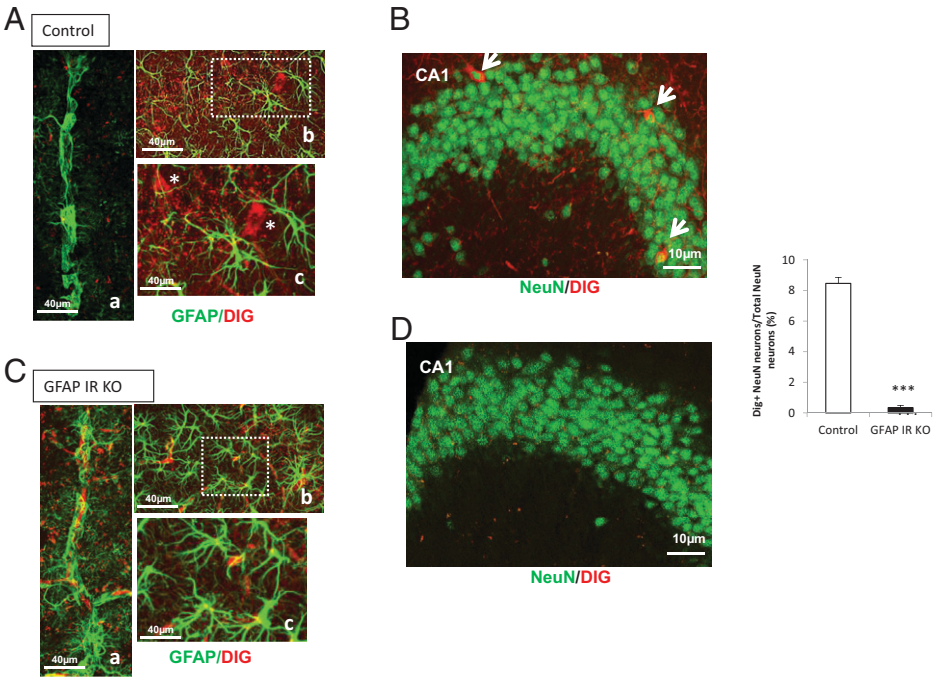

Fig. 3. Astrocytic IRs participate in brain transfer of peripheral insulin. (*A*) Double immunocytochemistry of Dig-Ins (DIG) and GFAP in somatosensorial cortex of littermate mice after intracarotid injection of Dig-Ins. *A* shows astrocyte end feet (GFAP$^+$) ensheathing brain capillaries in littermate (control) mice after Dig-Ins injections (n = 10). Dig staining is seen in cells of *b* (white dotted square) with neuronal morphology (red), which are magnified in *c* (white asterisks) (n = 10). (*B*) Dig-Ins in hippocampal granular layer neurons (NeuN$^+$ cells) of control mice (n = 10). (*C*) Double immunocytochemistry of DIG and GFAP in somatosensorial cortex of GFAP-IR KO mice after injection of Dig-insulin. *a* shows astrocyte end feet (GFAP$^+$) ensheathing brain capillaries in GFAP-IR KO mice after Dig-insulin injections (n = 10). In *b* and *c* (higher magnification of dotted white square in *b*) neuronal-like shapes with Dig staining are absent. (*D*) Hippocampal neurons in GFAP-IR KO mice do not show Dig staining (n = 10). Green, GFAP$^+$ or NeuN$^+$ cells; red, digoxigenin$^+$ cells. Histograms: quantification of Dig-labeled NeuN$^+$ cells in control and GFAP-IR KO mice (n = 10 per group, t test, ***$P < 0.001$).

GFAP astrocytes in GFAP-IR KO mice show a distinct activation-like morphology as compared to astrocytes in littermates.

Brain Insulin Resistance Uncouples Brain Flow and Glucose Uptake. Because young GFAP-IR KO mice have reduced brain glucose uptake, probably related to decreased glucose transporter 1 (GLUT1) levels in the brain (10) (*SI Appendix*, Fig. S2*C*), we determined their brain perfusion, as blood flow and glucose uptake may be linked through astrocytes (18), and insulin can affect endothelial function (1, 2). Moreover, reduced GLUT1 elicits compensatory increases of the angiogenic factor VEGF (19) that can promote vessel growth. Indeed, disturbed brain perfusion and glucose uptake go hand in hand in different brain pathologies.

We examined brain perfusion along time using single-photon emission computed tomography (SPECT) of 99mTc-D,L-hexamethylpropylene amine oxime (^{99}mTc-HMPAO) (20), as age-related changes in brain blood flow also relate to astrocyte activity (21). Young (~3 mo of age, *Upper* bars in Fig. 4*A*) GFAP-IR KO mice present significantly increased brain perfusion, while at later ages (>1-y-old "aged" mice, *Lower* bars) brain perfusion significantly decreased (**$P < 0.01$ vs. littermates, t test; Fig. 4*A*). Perfusion was altered along this age range only in GFAP-IR KO mice (**$P < 0.01$ vs. littermates, t test; *SI Appendix*, Fig. S3*A* and *B*) and depended on the timing of IR deletion, since when tamoxifen was given to aged GFAP-IR KO mice, no disturbances were seen (*SI Appendix*, Fig. S3*C*). Changes were specific for astrocytic IRs, as mice lacking astrocytic IGF-I receptors did not show altered brain perfusion (*SI Appendix*, Fig. S3*D*).

Changes in redox status may interfere with cellular uptake of ^{99}mTc-HMPAO (22). Because astrocytes lacking IR show changes in mitochondrial function compatible with increased generation of oxidative radicals (10), and astrocytes are the predominant cell type accumulating ^{99}mTc-HMPAO in brain (23), we determined levels of reactive oxygen species (ROS) in the brain of GFAP-IR KO mice. No significant increases ($P = 0.055$, n = 10, 11; two-tailed t test) were seen in brain ROS levels in young mice, whereas aged GFAP-IR KO mice show no changes as compared with vehicle-injected controls (*SI Appendix*, Fig. S3*E* and *F*). Since increased ROS reduces ^{99}mTc-HMPAO uptake (24), changes in ^{99}mTc-HMPAO uptake do not seem related to ROS levels.

Previously, we reported that GFAP-IR KO mice show reduced brain glucose uptake at a young age (10). Indeed, 18F-fluoro-2-deoxy-D-glucose positron emission tomography (^{18}FDG-PET) analysis confirmed decreased brain glucose uptake in young GFAP-IR KO mice (***$P < 0.001$, t test; Fig. 4*B*). However, in older GFAP-IR KO mice, brain glucose uptake was slightly increased as compared to control, vehicle-injected mice (Fig. 4*B*). Brain glucose uptake was significantly changed along this age range only in GFAP-IR KO mice, as their control littermates did not show significant changes along this time (*SI Appendix*, Fig. S3*G* and *H*). Collectively, these observations suggest that GFAP-IR KO mice have uncoupled brain blood flow and brain glucose uptake with a changing pattern along time.

IRs in Astrocytes Modulate Brain Angiogenesis. Since brain ^{99}mTc-HMPAO uptake is mostly reflecting its astrocyte accumulation and changes in astrocyte metabolism may interfere with this uptake (23), we determined brain vessel biomarkers to determine whether changes in ^{99}mTc-HMPAO uptake parallel changes in vascularity. Brain levels of von Willebrand factor (vWF), a marker of microvessel density (25), were increased in young, but not in adult GFAP-IR KO mice (*$P < 0.05$, t test; Fig. 5*A*), matching the observed age-dependent changes in brain perfusion (Fig. 4*A*). Further, morphometric evaluation of brain vessels in GFAP-IR KO mice confirmed increased vascularity in young but not older GFAP-IR KO mice (**$P < 0.01$, t test; Fig. 5*B*). Increased vascular density was present in young, but not aged GFAP-IR KO mice, compared to littermates (Fig. 5*B*, **$P < 0.01$), in agreement with the observed perfusion values (Fig. 4*A*). However, the myelin-associated glycoprotein (MAG)/proteolipid protein 1 (PLP1) ratio, a marker of white matter perfusion (26), remained unchanged in young mice (*SI Appendix*, Fig. S3*H* and I), suggesting that gray matter perfusion is specifically affected.

Furthermore, GFAP-IR KO mice showed time-dependent changes in brain levels of the hypoxia-inducible factor (HIF)

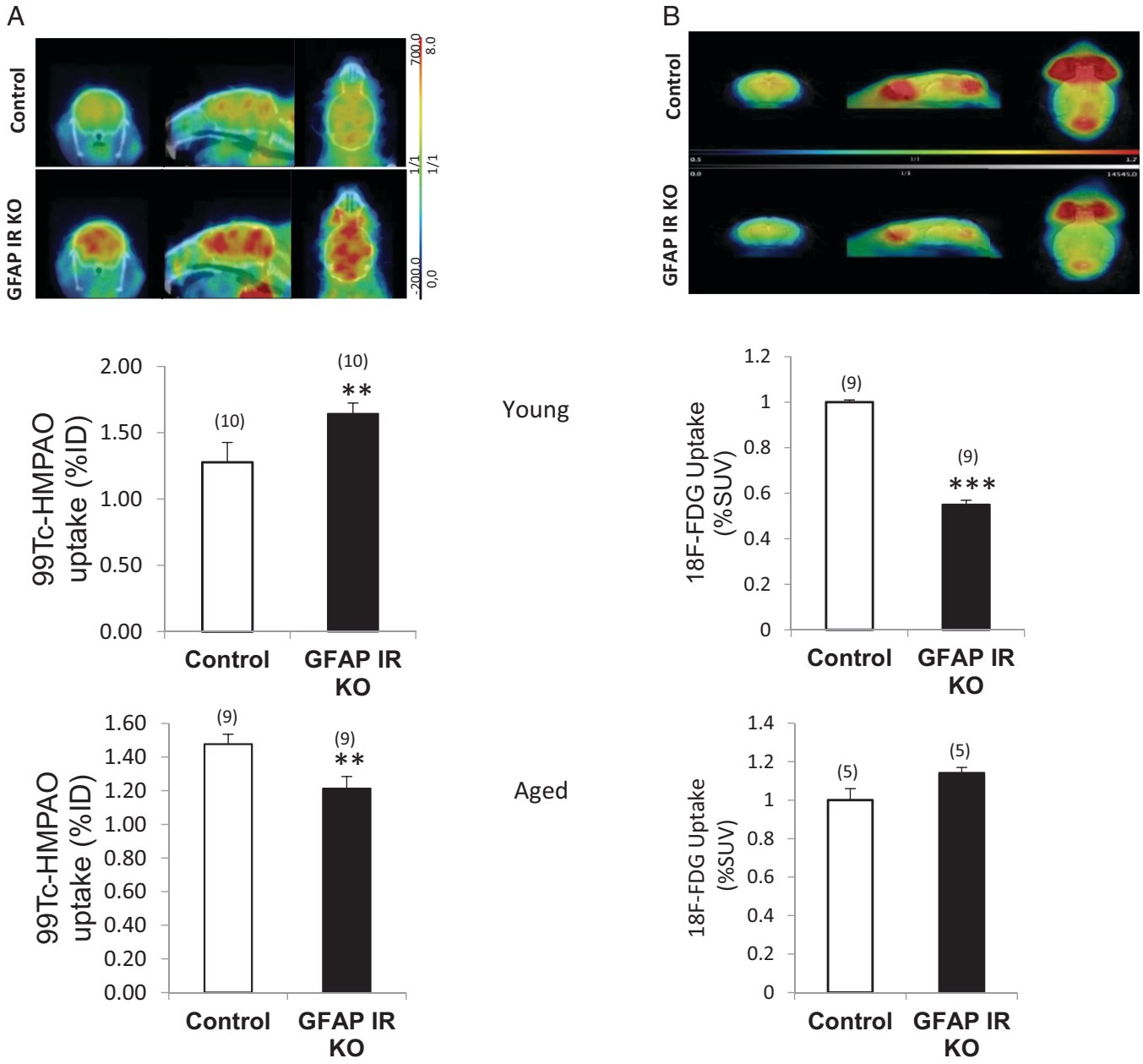

Fig. 4. Astrocytic IRs are involved in neurovascular coupling. (*A*) Brain perfusion, as determined by brain ^{99}mTc-HMPAO accumulation, in young (3 mo old, *Upper* histograms) and adult (>1 y old, *Lower* histograms), GFAP-IR KO mice and control littermates (n = 9 to 10 per group; t test, t = 2.95; $^{**}P < 0.01$). A representative SPECT image taken from young mice is shown. (*B*) Brain glucose uptake, as determined by ^{18}F-FDG, in young and adult GFAP-IR KO mice and littermates (n = 5 to 9 per group; t test, t = 3.64; $^{***}P < 0.001$). A representative PET image taken from young mice is shown.

1α/vascular endothelial growth factor (VEGF) angiogenic pathway, with increased expression in young mice and slightly reduced or normal in older mice ($^{*}P < 0.05$ and $^{***}P < 0.001$ vs. controls, t test; Fig. 5*C* and *D*). Furthermore, mRNA expression of angiogenic proteins such as transforming growth factor (TGF) β3, VEGFa/c, and estrogen-related receptor beta (Erb)-receptor tyrosine kinase 2 (ErbB2), was increased in young mice ($^{*}P < 0.05$, and $^{***}P < 0.001$, t test; *SI Appendix*, Fig. S4*A*), as determined by qPCR, whereas at later ages expression of these genes were either reduced or within control levels ($^{*}P < 0.05$, t test; *SI Appendix*, Fig. S4*B*). Other genes related to angiogenesis such as matrix metallopeptidase (Mmp)14 and prostaglandin-endoperoxide synthase (PTGS) 1 remained unaffected (*SI Appendix*, Fig. S4*C* and *D*). Further, expression of these angiogenic markers, including Mmp14 and PTGS1, was increased in the brain of young mice lacking IRs in tamoxifen-regulated glutamate/aspartate transporter (GLAST) astrocytes (GLAST-IR KO mice; *SI Appendix*, Fig. S5), that show a larger down-regulation of IRs in astrocytes (10). This confirms increased expression of angiogenic markers in the brain of young mice lacking IRs in either GFAP or GLAST astrocytes.

We then determined whether astrocytes are directly related to brain changes of angiogenic mediators in GFAP-IR KO mice. We reduced IR in astrocytes through two complementary methods, i.e., RNA interference (RNAi) in wild-type (WT) astrocytes or culturing of astrocytes from GFAP-IR KO mice. After reducing IR expression in WT astrocytes by short-hairpin RNA (sh-IR, Fig. 6*A* and *B*, *Lower* blots), levels of the angiogenic signals HIF1α and VEGF increased ($^{**}P < 0.01$, t test; Fig. 6*A* and *B*). This is accompanied by increased expression of VEGFa and TGFβ$_3$ ($^{*}P < 0.5$ and $^{**}P < 0.01$, t test; Fig. 6*C*), while other angiogenic signals, including VEGFc, PTGS1, MmP14, ErbB2, and vWF remained unaltered. Thus, several,

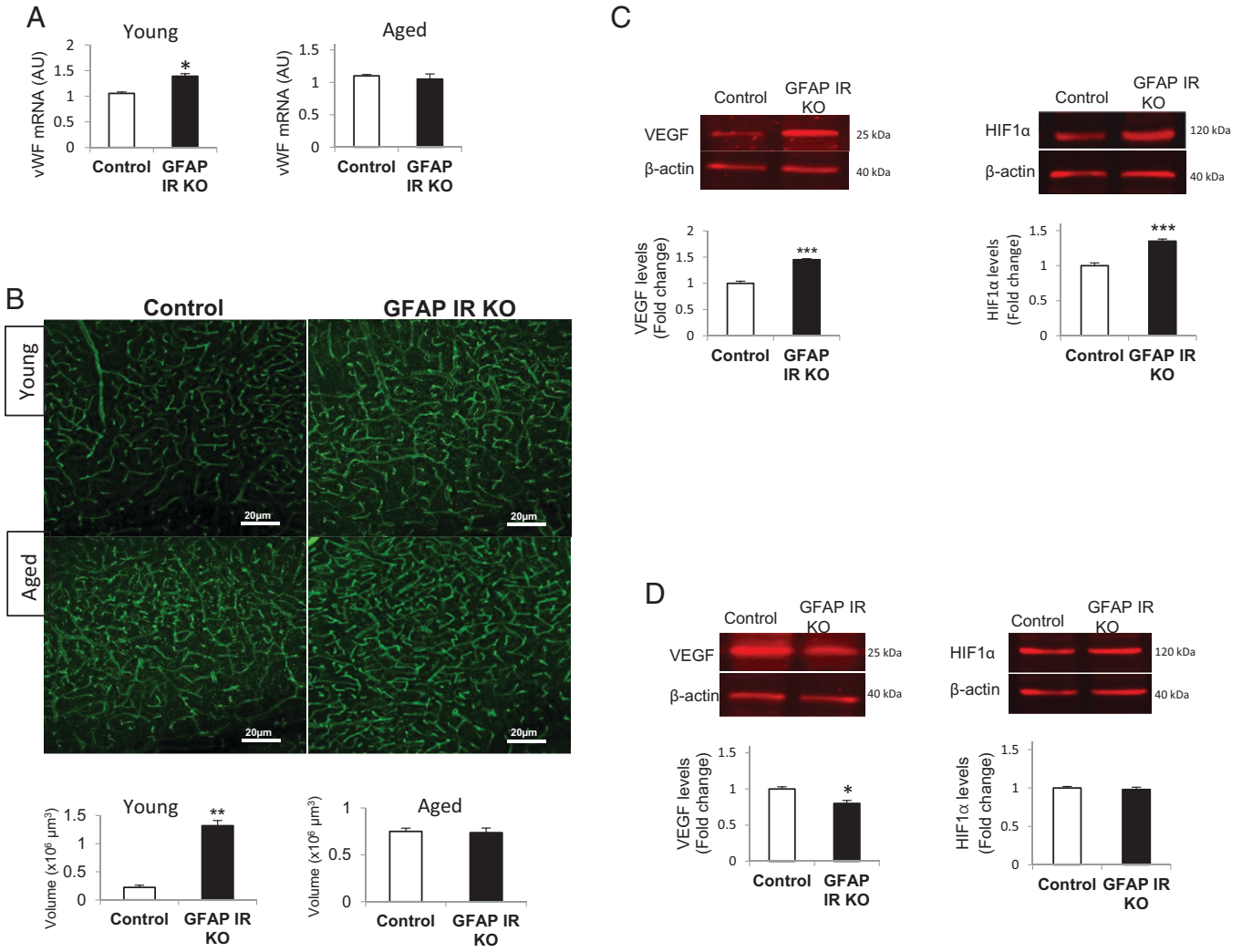

Fig. 5. Astrocytic IRs modulate brain angiogenesis. (*A*) Brain levels of vWF in young (*Left* histograms) and aged (*Right* histograms) GFAP-IR KO and littermate mice ($n = 10$; t test, t = 3.56, $^{*}P < 0.05$). (*B*) Vessel volume in the somatosensorial cortex of young (*Upper*) and aged (*Lower*) GFAP-IR KO mice and controls ($n = 9$; t test, t = 3.28, $^{**}P < 0.01$). Vessels were identified with Fluorescein isothiocyanate (FITC)-labeled tomato lectin and quantified (*Lower* histograms: *Left*, young mice and *Right*, older mice). (*C* and *D*) Protein levels of VEGFa and HIF-1α in young (*C*) and aged GFAP-IR KO mice and littermates (*D*) ($n = 9$; t test, t = 3.12, $^{*}P < 0.05$ and $^{***}P < 0.001$).

but not all the angionenic molecules altered in the brain were also changed in IR-deficient astrocytes. Conversely, insulin upregulates this pathway in wild-type astrocytes ($^{**}P < 0.01$, t test; *SI Appendix*, Fig. S6*A*). These observations agree with previously reported ligand-independent actions of IR (27), and hint to a key, complex role of insulin signaling on astrocytic angiogenic pathways.

Because reduced astrocytic IR function affects neurons (10), we determined whether its reduction also impacts brain endothelial cells, as astrocytes are in close contact with them and their growth and differentiation may be modulated by astrocyte-derived angiogenic signals (28). We used astrocytes obtained from GFAP-IR KO mice with reduced IR levels ($^{**}P < 0.01$, t test; *SI Appendix*, Fig. S6*B*) and cocultured them with wild-type endothelial cells. We observed that higher levels of angiogenic markers in cocultures of astrocytes lacking IR (HIF1α and VEGF, $^{**}P < 0.01$, t test; Fig. 6*D* and *E*), were accompanied by increased endothelial growth, as determined by higher levels of CD31, a marker of endothelial cells ($^{***}P < 0.01$, t test; Fig. 6*F*) or stronger CD31 immunostaining of WT endothelial cells cocultured with GFAP-IR KO astrocytes (Fig. 6*G*).

Since high glucose has been reported to interfere with the mitogenic activity of astrocytes on endothelial cocultures (29), we determined HIF1α/VEGF levels in astrocytes grown at different glucose concentrations and found glucose-dependent increases in both (*SI Appendix*, Fig. S6*C*). While young GFAP-IR KO mice show normal serum insulin levels (10), they are hyperglycemic ($^{*}P < 0.05$, t test; Fig. 7*A*), suggesting that higher glucose may contribute to the observed higher brain vascularity. Further, normalized brain glucose uptake in older GFAP-IR KO mice may also be related to prior exposure to hyperglycemia, which has been hypothesized to alter brain glucose transporters (30). Indeed, brain GLUT1 expression in aged GFAP-IR KO and GLAST-IR KO mice was higher than in young ones and within control levels (*SI Appendix*, Fig. S2*C*, *Right*), suggesting that early exposure to high glucose may underlie the recovery in GLUT1 levels and consequently in brain glucose uptake. However, in vitro exposure to 50 mM glucose increased expression of GLUT1 mRNA in control but not in GFAP-IR KO astrocytes ($^{***}P < 0.001$, t test; Fig. 7*B*). Thus, recovery of brain glucose uptake along time in the brain of GFAP-IR KO mice may involve other pathways.

IR Modulates Mitochondrial Function in Astrocytes. Since mitochondria modulate angiogenic signaling (31), and GFAP-IR

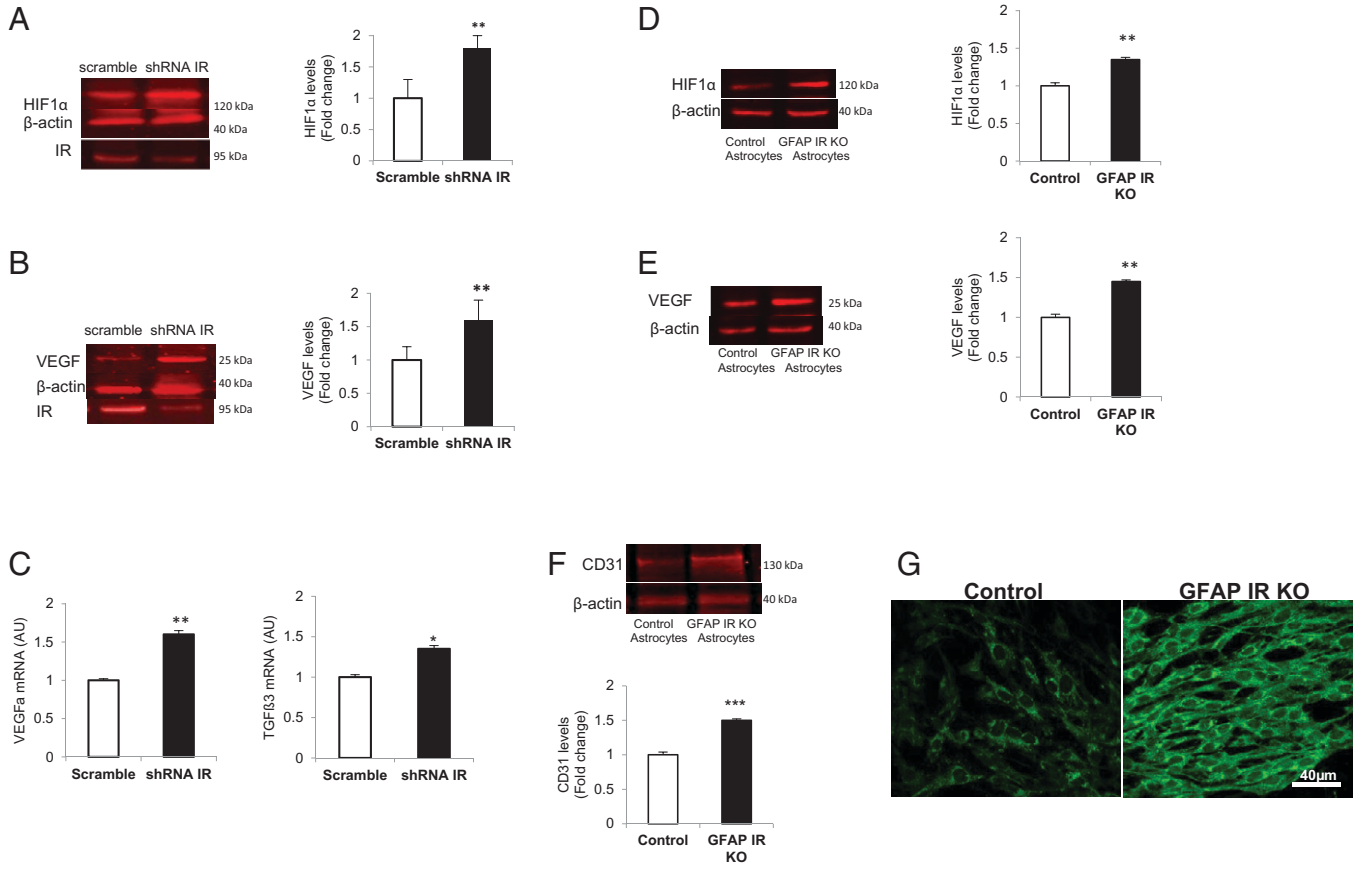

Fig. 6. Increased angiogenic signaling in IR-deficient astrocytes. (*A*) Levels of HIF1α in IR-deficient (shRNA IR) and control (scramble) astrocytes. Representative blot and quantitation histogram are shown. Actin is used to normalize protein load ($n = 9$; *t* test, t = 3.29, $^{**}P < 0.01$). (*B*) VEGFa levels in shRNA IR and scramble astrocytes ($n = 9$; *t* test, t = 3.53, $^{**}P < 0.01$). (*C*) Expression of VEGFa and TGFβ3 in shRNA IR and scramble astrocytes ($n = 9$; *t* test, t = 2.88, $^{*}P < 0.05$ and $^{**}P < 0.01$). (*D*) HIF1α levels in endothelial cells cocultured with GFAP-IR KO or control (littermate) astrocytes ($n = 9$; *t* test, t = 2.91, $^{**}P < 0.01$). (*E*) VEGFa levels in endothelial cells cocultured with GFAP-IR KO or control astrocytes ($n = 9$; *t* test, t = 3.09, $^{**}P < 0.01$). (*F*) CD31 levels in endothelial cells cocultured with GFAP-IR KO or control astrocytes ($n = 9$; *t* test, t = 3.02, $^{***}P < 0.001$). (*G*) CD31 staining in endothelial cells cocultured with GFAP-IR KO or control astrocytes.

KO mice show altered mitochondrial function in astrocytes (10), we examined whether increased angiogenesis in these mice is related to altered mitochondrial function. We determined levels of ROS in IR-deficient astrocytes using 2',7'-dichlorodihidrofluoresceín diacetate (H2DCFDA), a ROS-sensitive fluorescent dye, and found them increased as compared to control cultures (Fig. 7*C*). Next, we inhibited ROS with *N*-acetylcysteine (NAC; 10 mM) in IR-deficient astrocytes (Fig. 7*D*, compare *Right* and *Left* histograms) to determine its role in angiogenic signaling and found normalized HIF-1α/VEGF levels (Fig. 7*E* and *F*). These in vitro observations in shRNA IR-transfected astrocytes were confirmed in vivo. Treatment of young GFAP-IR KO mice with NAC (600 mg/kg, ip) normalized brain blood flow (Fig. 7*G*) and glucose uptake (Fig. 7*H*, compare with Fig. 4*B*, *Upper* bars), and increased brain γ-l-glutamyl-l-cysteinyl-glycine (GSH), an antioxidant defense metabolite found decreased in untreated mice ($^{**}P < 0.01$ and $^{***}P < 0.001$ vs. untreated GFAP-IR KO control mice, two-way ANOVA; Fig. 7*I*).

Increased ROS impairs mitochondrial function (32), whereas defective mitochondria are removed by mitophagy (33). Indeed, shRNA-transfected astrocytes showed a decreased mitofussin 2 (Mfn2)/Fis1 ratio, an indicator of increased mitophagy ($^{**}P < 0.01$, *t* test; Fig. 8*A*), and increased depolarized mitochondria ($^{**}P < 0.01$, *t* test; Fig. 8*B* and *SI Appendix*, Fig. S7*A*), an indicator of the preautophagic pool of dysfunctional mitochondria (34) as determined by the ratio of red/green JC1, a fluorescence sensor of mitochondrial membrane potential. ROS also stimulates mitochondria biogenesis (35), and mitophagy is coupled to this process (36). Indeed, IR-deficient astrocytes show increased expression of peroxisome proliferator–activated receptor-gamma coactivator-1alpha (PGC-1α), a marker of mitochondria biogenesis ($^{**}P < 0.01$, *t* test; Fig. 8*C*).

Since mitochondria endoplasmic reticulum (ER) contact sites (MERCs) in reactive astrocytes are involved in vascular remodeling (37), and astrocyte morphology in GFAP-IR KO mice resembles reactive astrocytes (10, 38), we analyzed MERC dynamics, since this region is responsible for the interaction between both organelles. We determined in IR-deficient astrocytes the assembly of the MERC complex formed by the chaperone glucose regulated protein 75 (GRP75) with inositol trisphosphate receptors (IP3R, located in the ER) and voltage-dependent anion channel (VDAC, located in the mitochondria). GRP75 tethers IP3R with VDAC and the resulting complex bridges both organelles and is involved in Ca^{2+} signaling (39). We used proximity ligation assays (PLAs) to determine the interaction of GRP75 with IP3R and of Grp75 with VDAC and in this way the degree of contact at the mitochondrial–ER junction (40). We found greatly decreased interaction between both pairs of proteins, indicating reduced interaction of the two organelles in IR-deficient astrocytes ($^{**}P < 0.01$, *t* test Fig. 8*D* and *E*). Collectively, mitochondrial activity seems impaired in IR-deficient astrocytes, which helps explain changes in vasculature.

To determine the impact of altered mitochondrial dynamics in angiogenic signaling/glucose handling by astrocytes lacking

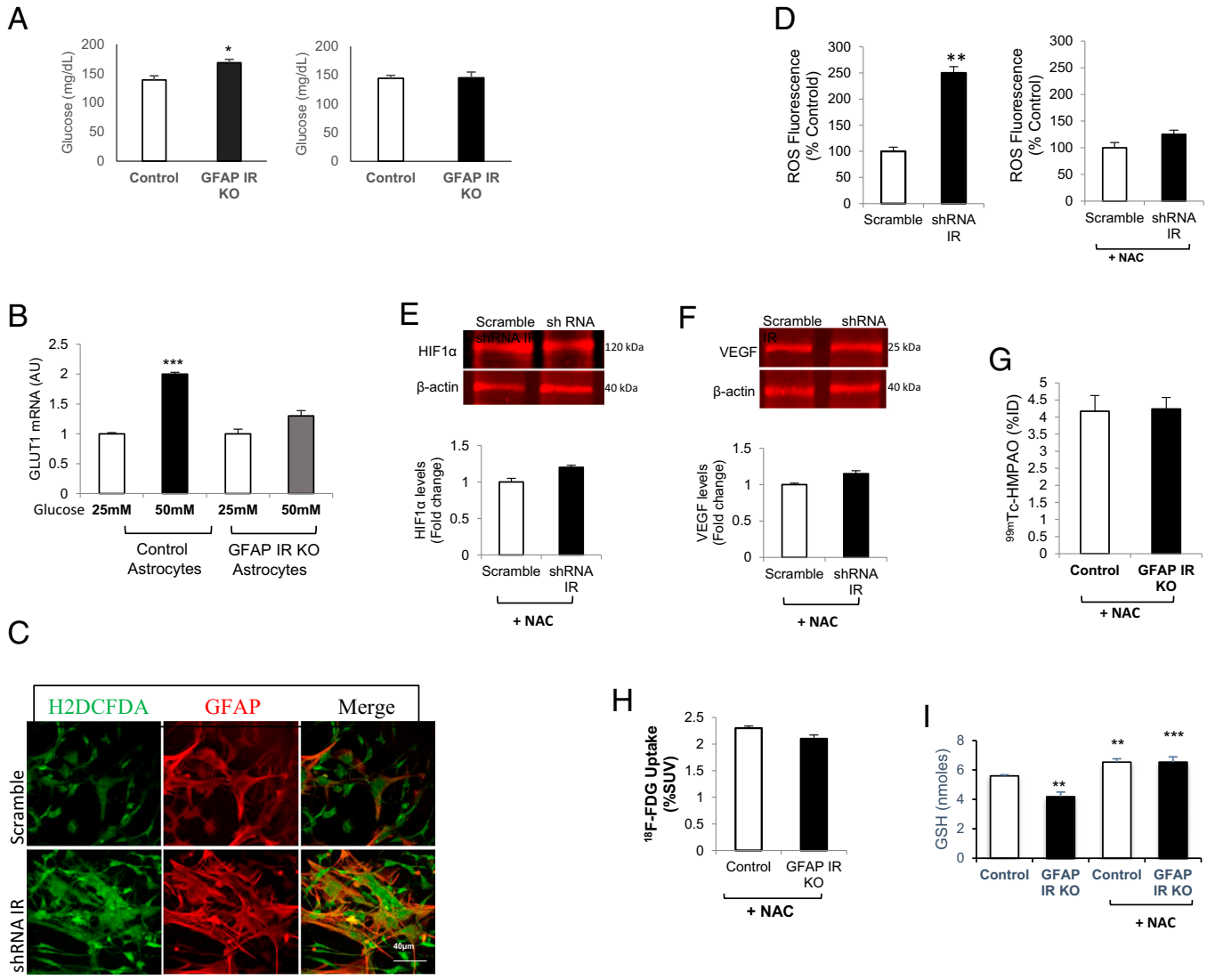

Fig. 7. Astrocyte IR deficiency affects glucose homeostasis and ROS production. (*A*) Blood glucose levels in young (*Left*) and aged (*Right*) GFAP-IR KO mice and littermates (n = 5 to 6 per group; t test, t = 3.66, $^{*}P < 0.05$). (*B*) GLUT1 mRNA levels in astrocytes from GFAP-IR KO mice and littermate controls (n = 9; two-way ANOVA, F = 10.36; $^{***}P < 0.001$). (*C*) Representative photomicrographs of astrocyte cultures (GFAP^{+} cells, in red) where ROS are detected using the fluorescent marker H2DCFDA (green). (*D*) ROS levels were quantified in astrocyte cultures treated or not with NAC after knockdown of IR (*SI Appendix*, Fig. S4*B*) (n = 9; t test, t = 3.49; $^{**}P < 0.01$). (*E* and *F*) HIF1α (*E*) and VEGF (*F*) levels in shRNA IR astrocytes and controls after NAC treatment. (*G* and *H*) Blood flow (*G*) and glucose uptake (*H*) in GFAP-IR KO mice and littermates treated with NAC (n = 9; $^{**}P < 0.01$). (*I*) GSH levels in the brain of GFAP-IR KO mice and littermates with or without NAC treatment (n = 8; two-way ANOVA, F = 10.31 $^{**}P < 0.01$ and $^{***}P < 0.001$ vs. untreated control mice).

IR, mitophagy was inhibited with cyclosporine (5 μM) (41), as indicated by a normalized Mfn2/Fis1 ratio in these cells (*SI Appendix*, Fig. S7*B*). Cyclosporine normalized HIF-1α/VEGF (*SI Appendix*, Fig. S7*C* and *D*) and GLUT1 (*SI Appendix*, Fig. S7*E*) levels in GFAP-IR KO astrocytes. Hence, disturbed mitochondrial function in astrocytes with down-regulated IR alters markers of angiogenic and glucose metabolism, suggesting that it underlies the observed changes in brain perfusion and glucose uptake.

Since mitochondria are involved in O_2 (42) and glucose (43) sensing, we next examined whether down-regulation of IR affects these two mechanisms in astrocytes, as they are also linked to angiogenesis and glucose uptake. We determined in GFAP-IR KO astrocytes the levels of transient receptor potential ankyrin 1 (TRPA1) channels ($^{**}P < 0.01$, t test; Fig. 9*A*) and of nicotinamide adenine dinucleotide phosphate (NADPH) ($^{**}P < 0.01$, t test; Fig. 9*B*), two O_2 sensors (44, 45) expressed in astrocytes. We also determined levels of the mitochondrial glucose sensor MondoA/Mlx, a transcription factor in the mitochondrial membrane involved in responses to glucose (43), and found it decreased in GFAP-IR KO astrocytes ($^{**}P < 0.01$, t test; Fig. 9*C*). Amelioration of ROS levels with NAC also resulted in normalization of TRPA1, NADPH, and MondoA levels (Fig. 9*A*–*C*). This suggests that excess ROS is involved in decreased levels of O_2 and glucose sensors in IR-defective astrocytes, which probably contributes to altered brain perfusion and glucose uptake.

Discussion

These observations indicate that insulin receptors in astrocytes modulate neurovascular coupling by modulating brain glucose uptake and vascular function (Fig. 9*D*). Mice with insulin receptor deficiency in astrocytes have been previously shown to display central and peripheral deficiencies in glucose metabolism and gliotransmission (10, 46). The present observations provide additional evidence that insulin signaling in this type of glial cells is important for brain function. Mice with IR deficiency in astrocytes

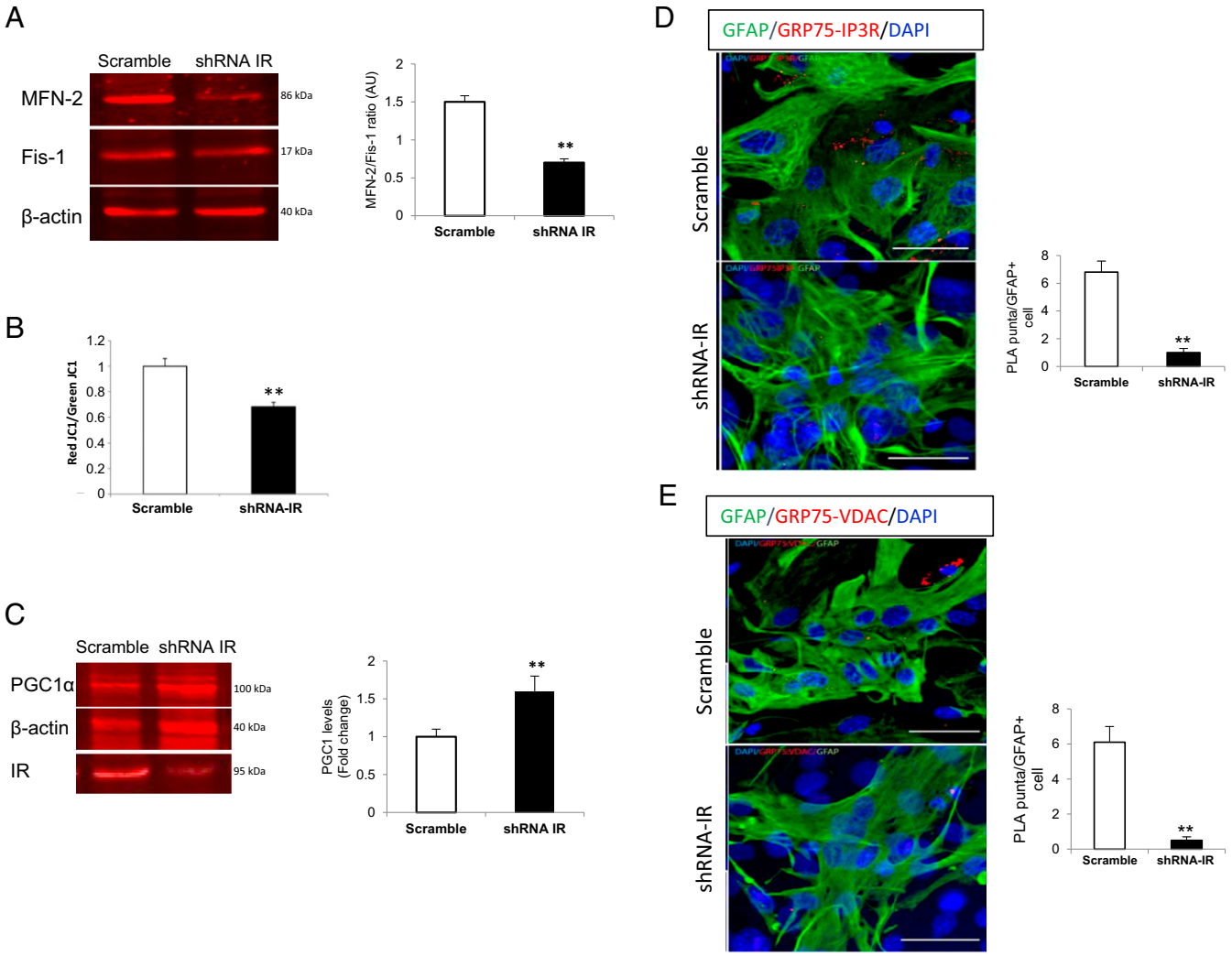

Fig. 8. Altered mitochondrial dynamics in IR-deficient astrocytes. (*A*) Mitofusin 2 (Mfn2, a marker of mitochondrial fusion) and fissin1 (Fis1, a marker of mitochondrial fission) ratio in shRNA IR and scramble astrocytes ($n = 9$; *t* test, t = 3.06; $^{**}P < 0.01$). (*B*) Relative quantification of mitochondrial depolarization using the mitochondrial membrane potential fluorescence indicator JC1 (red/green JC1 ratio) in scramble ($n = 3$) and shRNA IR ($n = 8$) cultures (two-tail *t* test, t = 3.77; $^{**}P < 0.01$). (*C*) PGC-1α levels in shRNA IR and scramble astrocytes ($n = 9$; *t* test, t = 3.50; $^{**}P < 0.01$). (*D* and *E*) Interactions of GFP75 with IP3R (*D*) ($n = 7$; *t* test, t = 3.75; $^{**}P < 0.01$) and VDAC (*E*) revealed by PLA ($n = 9$; *t* test, t = 3.48; $^{**}P < 0.01$). Representative images are shown from scramble and shRNA IR astrocytes ($GFAP^+$ cells, green). Histograms show the ratio of PLA puncta per $GFAP^+$ cell. Nuclei staining is with DAPI. (Scale bars, 40 μm.)

develop brain insulin resistance, as previous results suggested (10), together with uncoupled brain blood flow and glucose uptake.

We also observed disturbed mitochondrial function in astrocytes with down-regulated IR signaling, which is associated with excess ROS production. Mitochondrial disturbances involved not only previously documented structural and metabolic alterations (10), but also led to impaired mitochondrial biogenesis, reduced levels of glucose/O_2 sensors, and decreased mitochondrial ER contacts (that ultimately affect astrocyte Ca^{2+} signaling). The latter was also observed in proopiomelanocortin (POMC) neurons of these mice (10). When high ROS levels or aberrant mitophagy are pharmacologically ameliorated, mitochondrial function is restored. Our findings describe a role for mitochondrial astrocytes in the purported relationship between cerebral blood flow and brain metabolism (18) and further substantiate brain blood flow disturbances in insulin-resistant states (5).

The presence of IR in astroglial end feet, similar to previous observations with the closely related insulin-like growth factor I receptor (47), provides anatomical support for its actions on the vasculature, as glial end feet are intricately participating in neurovascular coupling (48). Anatomically, large bundles of glial end-feet mitochondria are in close proximity to vessels (49), assuring local metabolic support (50), and, as our results now suggest, angiogenic signals. Changes in mitochondrial morphology and increased autophagic-related organelles in astrocytes lacking IR were previously observed (10). Conceivably, altered angiogenic signaling in GFAP-IR KO mice may be the result of altered mitochondrial function, as mitochondria modulate angiogenesis (31). In agreement with angiogenic actions of astrocytic IR, changes in angiogenic signaling are proportional to the degree of reduction in astrocyte IR, i.e., its deletion in GLAST astrocytes that constitute a larger population of astrocytes compared to GFAP astrocytes (10), produces a larger increase in angiogenic signaling compared to knockdown of IR in GFAP astrocytes. Further, IR in pericytes has been reported to control retinal vasculature (2). Thus, IRs in BBB cells regulate vessel function.

An intriguing aspect of our observations is the evolving pattern of glucose/blood flow uncoupling along time. While observations of neurovascular uncoupling of brain glucose uptake and perfusion along aging in humans are confusing (51), a contribution of astrocytes has been recognized (21). Instances of uncoupling have been documented under physiological conditions in experimental

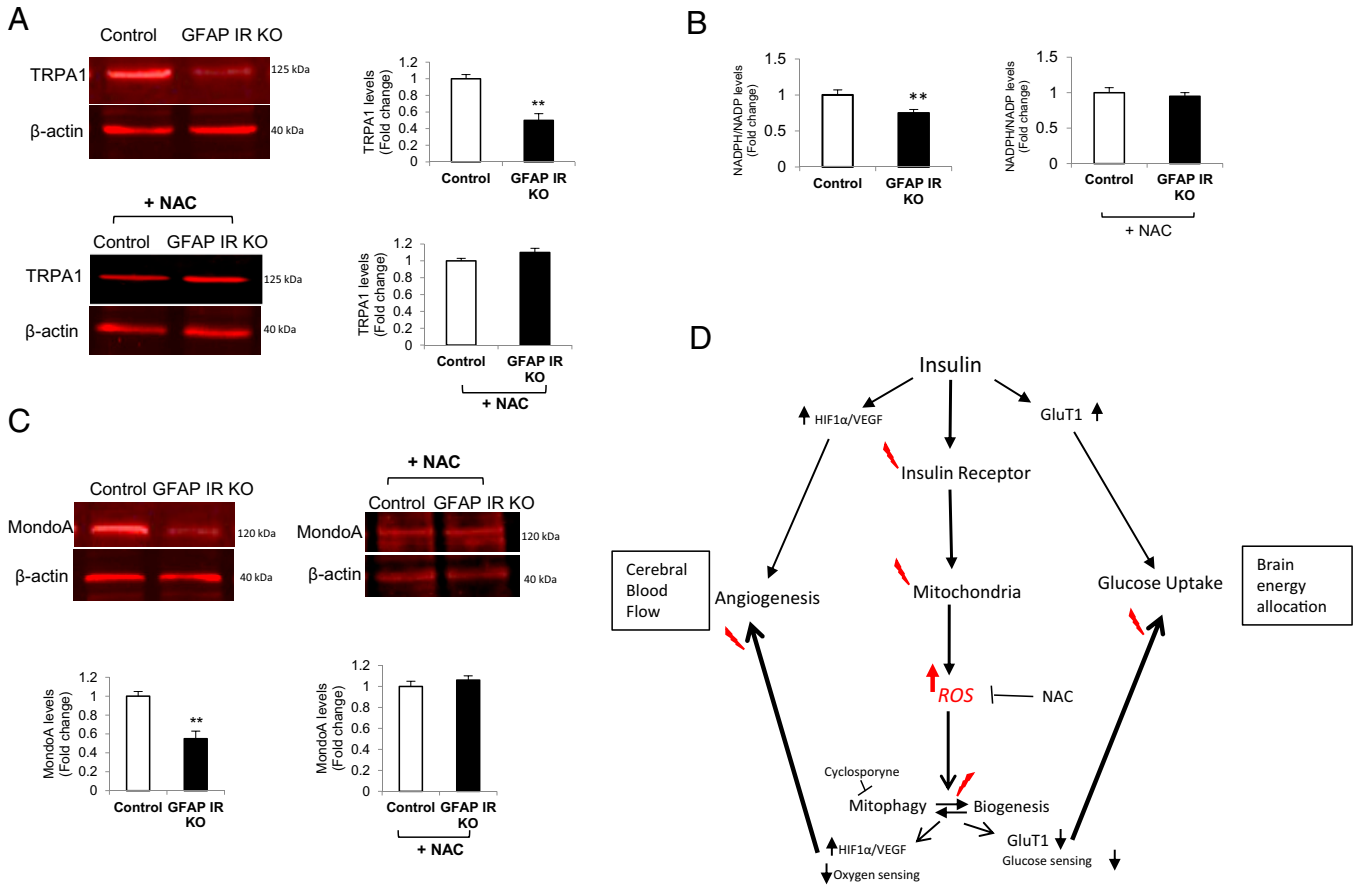

Fig. 9. Altered glucose/oxygen sensing in IR-deficient astrocytes. (*A*) TRPA1 levels in GFAP-IR KO and control astrocytes (*Upper*) and after treatment with NAC (*Lower*, $n = 9$; *t* test, t = 3.45; $^{**}P < 0.01$). (*B*) NADPH levels in GFAP-IR KO and control astrocytes (*Upper* histograms) and after NAC treatment (*Lower* histograms, $n = 9$; *t* test, t = 3.52; $^{**}P < 0.01$). (*C*) Levels of MondoA in GFAP-IR KO and control astrocytes (*Left*) and in cultures treated with NAC (*Right*) ($n = 9$; *t* test, t = 3.03; $^{**}P < 0.01$). Representative blots and quantitation histograms are shown. (*D*) Summary of observations of this study. Insulin signaling in astrocytes participates in neurovascular coupling (allocation of resources in conjunction with brain perfusion) by modulating angiogenic signaling/oxygen sensing and glucose uptake/sensing through mitochondrial-dependent mechanisms. Disruption (red saw symbol) of IR activity in astrocytes originates excess local levels of ROS that affect mitochondrial dynamics (including MERCs and Ca^{2+} handling), resulting in disruption of angiogenic balance and glucose uptake. Pharmacological amelioration of mitochondrial activity restores neurovascular coupling.

animals (52). These authors observed increased glucose uptake in the face of reduced brain perfusion and invoked mediators produced by BBB cells (52). Thus, neurovascular coupling cannot solely be explained as an energy-driven process.

A potential explanation of time-dependent changes in the observed uncoupling is that protracted impairment of central and peripheral glucose handling in GFAP-IR KO mice may gradually wear off aberrant angiogenic signaling by astrocytes. Alternatively, sustained mitochondrial injury in the brain of GFAP-IR KO mice due to excess ROS in astrocytes, may eventually result in loss of angiogenic potential. In turn, reduced perfusion in older GFAP-IR KO mice is accompanied by slightly increased glucose uptake, a common adaptive mechanism seen in humans.

Of note, ApoE4 carriers show a similar age-dependent change in brain perfusion, with higher levels in young adults and lower levels in older individuals (53). Since ApoE4 has been shown to interfere with insulin signaling (54), we speculate that the mechanism underlying age-dependent disturbed brain perfusion in ApoE4 carriers may be impaired IR activity in astrocytes. This possibility will require further study. Conversely, uncoupling between brain perfusion and glucose metabolism has been reported in prodromal stages of AD (55), and both processes decay in parallel along progression of the disease (56). Since there is growing awareness that AD is a syndrome arising from different pathogenic processes, we hypothesize that brain insulin resistance due to impaired astrocytic IR function may contribute to pathology in specific subtypes of AD. Again, this will require further study.

Although circulating insulin plays many important roles in the brain (57), the key question of how it reaches its numerous brain targets remains not entirely defined yet (15, 58). Early observations documented the presence of insulin in the cerebrospinal fluid (CSF) and in the brain (59, 60). Just relatively recently, the origin of brain insulin has been reasonably settled (61), including not only a peripheral source, but also low local production (62). Thus, for many years, insulin actions in the brain were assumed to arise exclusively from pancreatic insulin (63) that has to cross the BBB to exert its central actions. Indeed, circulating insulin enters the brain through a saturable transport mechanism (64). Whether the insulin receptor in endothelial cells is involved in the process remains controversial, as conflicting results have been published (15, 58, 65). There are insulin receptors in epithelial cells in the blood–CSF barrier at the choroid plexus (66), brain capillary endothelial cells of the BBB (67) able to transcytose insulin (68) and astrocytes (69). Our results suggest that astrocytes act as a gateway for circulating insulin into the brain, as previously hinted (10). Once insulin crosses the vessels, it can be carried by the glymphatic system, travel through the interstitial space, and/or be taken up by astrocytes. Thus, circulating insulin may reach its

neuronal targets through these different intracerebral pathways. Knowledge of the entire route of entrance of circulating insulin into the brain, including vessel transcytosis, is of great relevance, as in diabetes and in several neurodegenerative diseases, brain insulin resistance is a likely pathogenic component. Our results pose astrocytic IRs as important targets for future studies in the search of novel therapeutic options for brain insulin resistance. Indeed, GFAP-IR KO mice develop brain insulin resistance, as attested by blunted brain IR activation, reduced capture of circulating insulin, and loss of astrocyte responses to systemic insulin.

This study contains several limitations. For instance, both the PET and SPECT radiotracers used in this study are redox sensitive (24), which could interfere with the interpretation of changes in glucose uptake and blood flow, respectively. However, increased oxidative stress is associated with increased PET and decreased SPECT signal, respectively (24), making it unlikely that the observed decreased PET and increased SPECT signatures observed are related to increased brain ROS levels. Changes in SPECT and PET signatures correlated with angiogenic markers and GLUT1 levels, respectively, providing additional support to the validity of the measurements. Another limitation of the study is that we did not determine possible compensatory expression of IR (and even the closely related IGF1R) in other types of brain cells, which could contribute to the observed changes.

In summary, brain insulin resistance associates with increased ROS production and mitochondrial disturbances and interferes with functional hyperemia, resembling changes seen during brain aging. These results add to the multitasking role of astrocytic IRs, including regulation of peripheral glucose metabolism (70), gliotransmission, dopaminergic activity, mood homeostasis (46), and control of gonadal function (71). Boosting IR function in astrocytes may be of therapeutic value in neurodegenerative diseases with altered tissue perfusion and hypometabolism.

Materials and Methods

Detailed methods are included in *SI Appendix*.

Animals. Wild-type 6-mo-old male mice (C57BL6/J) and mutant mice with insulin receptors ablated in GFAP (GFAP-IR KO mice) or GLAST astrocytes (GLAST-IR KO mice) under regulation of tamoxifen were generated as described in detail before (10). Mice with IGF-I receptors ablated in GFAP astrocytes under the regulation of tamoxifen were obtained as indicated in *SI Appendix*. Intraperitoneal injection of tamoxifen for 5 consecutive days (75 mg/kg) to young mice (4 to 5 wk old) eliminated IR or IGF1R specifically in astrocytes, as reported (10).

Ca^{2+} Imaging. Chronic glass-covered cranial windows were implanted (Fig. 2*A*). A stereotaxic microinjection (400 nL; 30 nL/min) of AAV2/5-P_{GFAP}-Lck-GCaMP6f (PENN Vector Core; viral titer 6.13×10^{13}) was made. Imaging of GCaMP6f-expressing astrocytes was performed with a two-photon laser scanning microscope, custom-modified with a femtosecond laser (Chameleon Ultra II, Coherent, Inc.) and ScanImage 3.8 software written in MATLAB (MathWorks; RRID:SCR_001622), under isoflurane anesthesia (1 to 1.5%).

Cell Cultures and Transfections. Cultures were done as previously described in detail (72). For transfection, astrocytes were electroporated (2×10^6 astrocytes with 2 μg of plasmid DNA) before seeding, using an astrocyte Nucleofector Kit (Amaxa, Lonza).

Immunofluorescence. Immunolabeling was performed as described (73).

PLAs. Assays were run using the Duolink In Situ Detection Reagents Red Kit (DUO92008, Merck) as described (74).

NAC Administration. Six-week-old control littermates and GFAF IR KO mice were given a 1% solution of *N*-acetyl-L-cysteine in the drinking water (pH 7.2, Sigma) for a period of 4 mo. Then, mice were submitted for SPECT and PET analysis. Later, mice were killed and brain GSH content was measured.

For cell cultures, NAC was used at 10 mM for 24 h followed by different biochemical determinations.

Immunoprecipitation and Western Blotting. Assays were performed as described (75).

Immunoelectron Microscopy. Immunogold procedure was performed as described (76).

SPECT/CT Imaging. Mice were intravenously (i.v.) injected with ^{99}mTc-HMPAO (Curium Pharma) in a volume of 0.2 mL. An ISOMED 2010 dose calibrator was used to calibrate radiotracer doses. Thirty minutes after the injection of the radiotracer (32 to 42 MBq) SPECT and CT images were acquired with a bimodal Albira SPECT/CT preclinical imaging system (Bruker). Activity was quantified by matching the CT image of the skull of each animal to a common magnetic resonance (MR) mouse brain template, in which regions of interest (ROI) were previously delineated, as described elsewhere (77). ROI activity uptake was expressed as the percentage injected activity (%ID).

^{18}F-FDG PET Imaging. ^{18}F-FDG PET was used to measure brain glucose handling as described in detail before (78). ^{18}F-FDG uptake in the different brain regions was calculated in kBq/cc units.

ROS Imaging. Brain ROS levels were visualized following previously published procedures with some modifications (79) (*SI Appendix*).

Biochemical Assays. The NADPH/NADP ratio in astrocytes was calculated using a fluorometric NADP/NADPH assay (Abcam, ab176724). ROS levels in shRNA transfected astrocytes was determined using the fluorescent H2DCFDA (Invitrogen, D399) ROS indicator as described (80). GSH levels in GFAP-IR KO astrocytes were assessed using a fluorimetric glutathione assay (Sigma, CS1020) according to the manufacturer's instructions.

JC-1 Flow Cytometry. Astrocytes were nucleofected with IR siRNA or siRNA scramble as control and grown in normal conditions. Side scatter analysis and propidium iodide were used to discard death cells and gate selection.

Statistics. Data were analyzed with GraphPad Prism 8.0 software. Normality was verified using the Kolmogorov–Smirnov test. Student's *t* test was used for comparison of two groups, or one- or two-way ANOVA for comparison of more than two groups with a Bonferroni post hoc analysis. For nonnormally distributed data, we used the Kruskal–Wallis test followed by the Wilcoxon test.

Data Availability. All study data are included in the article and/or supporting information. The data has not been deposited in a public database.

ACKNOWLEDGMENTS. We are thankful to M. Garcia and R. Cañadas for technical support. This work was funded by Centro de Investigacion Biomedica en Red de Enfermedades Neurodegenerativas (CIBERNED) (Instituto de Salud Carlos III, Spain) to I.T.A., A.G., and T.I.; an Inter-CIBER project (PIE14/00061) to I.T.A. that forms part of the projects PID2019-104376RB-I00 (I.T.A.) and RTI2018-094887-B-I00 (M.N.) funded by MCIN/AEI/10.13039/501100011033; a grant from Junta de Andalucia Consejería de Economía y Conocimiento (P18-RT-2233 to A.G.) cofinanced by Programa Operativo FEDER 2014–2020; a grant from Instituto de Salud Carlos III Spain (cofinanced by FEDER funds from the European Union; PI21/00915 to A.G.); Grant PID2020-115218RB-I00 to T.I. funded by Ministerio de Ciencia e Innovacion/Agencia Española de Investigación (MCIN/AEI/10.13039/501100011033); and a grant from Comunidad de Madrid through the European Social Fund (ESF)–financed programme Neurometabolismo-Comunidad de Madrid (NEUROMETAB-CM) (B2017/BMD-3700 to I.T.A. and T.I.). M.N. was also supported by the Spanish Ministry of Science and Innovation (Ramón y Cajal RYC-2016-20414). J.P.-U. was contracted by CIBERNED.

Author affiliations: [a]Dept Systems and Functional Neuroscience. Cajal Institute, Consejo Superior de Investigaciones Cientificas, Madrid, E 28002 Spain; [b]Ciberned, Madrid, Spain; [c]Laboratory of Novel Targets in Neurodegeneration and Neuroprotection. Instituto de Investigaciones Biomédicas "Alberto Sols". Consejo Superior de Investigaciones Cientificas- Universidad Autonoma de Madrid, Madrid, E 28029 Spain; [d]Department of Cell Biology, Genetics and Physiology, Instituto de Investigación

Biomédica de Malaga (IBIMA), Faculty of Sciences, University of Malaga, Malaga, E 29590 Spain; [e]Dept Biochemistry and Molecular Biology. Faculty of Experimental Sciences, Universidad Francisco de Vitoria; Madrid, E 28223 Spain; [f]Neuroscience Program, Tulane University School of Science and Engineering, New Orleans, LA 70118-5698; [g]Astrocyte Biology Unit. Institute for Diabetes and Obesity, Munich, D-85764 Germany; [h]Laboratory of Neurobiology of Insulin Peptides. Achucarro Basque Center for Neuroscience, Leioa, E-48940 Spain; and [i]Ikerbasque Basque Science Foundation, Bilbao, E 48011 Spain

1. C. Zheng, Z. Liu, Vascular function, insulin action, and exercise: An intricate interplay. *Trends Endocrinol. Metab.* **26**, 297–304 (2015).
2. N. Warmke *et al.*, Pericyte insulin receptors modulate retinal vascular remodeling and endothelial angiopoietin signaling. *Endocrinology* **162**, bqab182 (2021).
3. V. Novak *et al.*, Enhancement of vasoreactivity and cognition by intranasal insulin in type 2 diabetes. *Diabetes Care* **37**, 751–759 (2014).
4. R. Muniyappa, J. R. Sowers, Role of insulin resistance in endothelial dysfunction. *Rev. Endocr. Metab. Disord.* **14**, 5–12 (2013).
5. H. Rusinek *et al.*, Cerebral perfusion in insulin resistance and type 2 diabetes. *J. Cereb. Blood Flow Metab.* **35**, 95–102 (2015).
6. P. R. Angelova *et al.*, Functional oxygen sensitivity of astrocytes. *J. Neurosci.* **35**, 10460–10473 (2015).
7. N. Marina *et al.*, Brain metabolic sensing and metabolic signaling at the level of an astrocyte. *Glia* **66**, 1185–1199 (2018).
8. C. Iadecola, The neurovascular unit coming of age: A journey through neurovascular coupling in health and disease. *Neuron* **96**, 17–42 (2017).
9. C. S. Roy, C. S. Sherrington, On the regulation of the blood supply of the brain. *J. Physiol.* **11**, 85–108, 17 (1890).
10. C. García-Cáceres *et al.*, Astrocytic insulin signaling couples brain glucose uptake with nutrient availability. *Cell* **166**, 867–880 (2016).
11. K. Kacem, P. Lacombe, J. Seylaz, G. Bonvento, Structural organization of the perivascular astrocyte endfeet and their relationship with the endothelial glucose transporter: A confocal microscopy study. *Glia* **23**, 1–10 (1998).
12. P. Fraisl, M. Mazzone, T. Schmidt, P. Carmeliet, Regulation of angiogenesis by oxygen and metabolism. *Dev. Cell* **16**, 167–179 (2009).
13. P. Toth, S. Tarantini, A. Csiszar, Z. Ungvari, Functional vascular contributions to cognitive impairment and dementia: Mechanisms and consequences of cerebral autoregulatory dysfunction, endothelial impairment, and neurovascular uncoupling in aging. *Am. J. Physiol. Heart Circ. Physiol.* **312**, H1–H20 (2017).
14. A. Ruitenberg *et al.*, Cerebral hypoperfusion and clinical onset of dementia: The Rotterdam Study. *Ann. Neurol.* **57**, 789–794 (2005).
15. S. M. Gray, K. W. Aylor, E. J. Barrett, Unravelling the regulation of insulin transport across the brain endothelial cell. *Diabetologia* **60**, 1512–1521 (2017).
16. T. Sartorius *et al.*, The brain response to peripheral insulin declines with age: A contribution of the blood-brain barrier? *PLoS One* **10**, e0126804 (2015).
17. Z. Ma, T. Stork, D. E. Bergles, M. R. Freeman, Neuromodulators signal through astrocytes to alter neural circuit activity and behaviour. *Nature* **539**, 428–432 (2016).
18. R. C. Koehler, R. J. Roman, D. R. Harder, Astrocytes and the regulation of cerebral blood flow. *Trends Neurosci.* **32**, 160–169 (2009).
19. A. Jais *et al.*, Myeloid-cell-derived VEGF maintains brain glucose uptake and limits cognitive impairment in obesity. *Cell* **165**, 882–895 (2016).
20. I. Apostolova *et al.*, Brain perfusion SPECT in the mouse: Normal pattern according to gender and age. *Neuroimage* **63**, 1807–1817 (2012).
21. S. Tarantini, C. H. T. Tran, G. R. Gordon, Z. Ungvari, A. Csiszar, Impaired neurovascular coupling in aging and Alzheimer's disease: Contribution of astrocyte dysfunction and endothelial impairment to cognitive decline. *Exp. Gerontol.* **94**, 52–58 (2017).
22. M. R. Jacquier-Sarlin, B. S. Polla, D. O. Slosman, Oxido-reductive state: The major determinant for cellular retention of technetium-99m-HMPAO. *J. Nucl. Med.* **37**, 1413–1416 (1996).
23. S. Zerarka, L. Pellerin, D. Slosman, P. J. Magistretti, Astrocytes as a predominant cellular site of (99m)Tc-HMPAO retention. *J. Cereb. Blood Flow Metab.* **21**, 456–468 (2001).
24. G. Maulucci *et al.*, Imaging reactive oxygen species-induced modifications in living systems. *Antioxid. Redox Signal.* **24**, 939–958 (2016).
25. T. Thomas, S. Miners, S. Love, Post-mortem assessment of hypoperfusion of cerebral cortex in Alzheimer's disease and vascular dementia. *Brain* **138**, 1059–1069 (2015).
26. R. Barker *et al.*, Pathophysiology of white matter perfusion in Alzheimer's disease and vascular dementia. *Brain* **137**, 1524–1532 (2014).
27. J. Boucher *et al.*, A kinase-independent role for unoccupied insulin and IGF-1 receptors in the control of apoptosis. *Sci. Signal.* **3**, ra87 (2010).
28. M. Cohen-Salmon *et al.*, Astrocytes in the regulation of cerebrovascular functions. *Glia* **69**, 817–841 (2021).
29. S. Cohen *et al.*, High glucose conditioned neonatal astrocytes results in impaired mitogenic activity in cerebral microvessel endothelial cells in co-culture. *Heliyon* **5**, e01795 (2019).
30. L. L. Leão *et al.*, Does hyperglycemia downregulate glucose transporters in the brain? *Med. Hypotheses* **139**, 109614 (2020).
31. A. Reichard, K. Asosingh, The role of mitochondria in angiogenesis. *Mol. Biol. Rep.* **46**, 1393–1400 (2019).
32. P. H. Willems, R. Rossignol, C. E. Dieteren, M. P. Murphy, W. J. Koopman, Redox homeostasis and mitochondrial dynamics. *Cell Metab.* **22**, 207–218 (2015).
33. G. Twig, O. S. Shirihai, The interplay between mitochondrial dynamics and mitophagy. *Antioxid. Redox Signal.* **14**, 1939–1951 (2011).
34. S. P. Elmore, T. Qian, S. F. Grissom, J. J. Lemasters, The mitochondrial permeability transition initiates autophagy in rat hepatocytes. *FASEB J.* **15**, 2286–2287 (2001).
35. T. Wenz, Regulation of mitochondrial biogenesis and PGC-1α under cellular stress. *Mitochondrion* **13**, 134–142 (2013).
36. K. Palikaras, E. Lionaki, N. Tavernarakis, Coordination of mitophagy and mitochondrial biogenesis during ageing in *C. elegans*. *Nature* **521**, 525–528 (2015).
37. J. Göbel *et al.*, Mitochondria-endoplasmic reticulum contacts in reactive astrocytes promote vascular remodeling. *Cell Metab.* **31**, 791–808.e8 (2020).
38. C. Escartin *et al.*, Reactive astrocyte nomenclature, definitions, and future directions. *Nat. Neurosci.* **24**, 312–325 (2021).
39. G. Szabadkai *et al.*, Chaperone-mediated coupling of endoplasmic reticulum and mitochondrial Ca^{2+} channels. *J. Cell Biol.* **175**, 901–911 (2006).
40. E. Tubbs, J. Rieusset, Study of endoplasmic reticulum and mitochondria interactions by in situ proximity ligation assay in fixed cells. *J. Vis. Exp.* **118**, 54899 (2016).
41. L. Esteban-Martínez *et al.*, Programmed mitophagy is essential for the glycolytic switch during cell differentiation. *EMBO J.* **36**, 1688–1706 (2017).
42. R. B. Hamanaka, N. S. Chandel, Mitochondrial reactive oxygen species regulate hypoxic signaling. *Curr. Opin. Cell Biol.* **21**, 894–899 (2009).
43. C. A. Stoltzman *et al.*, Glucose sensing by MondoA:Mlx complexes: A role for hexokinases and direct regulation of thioredoxin-interacting protein expression. *Proc. Natl. Acad. Sci. U.S.A.* **105**, 6912–6917 (2008).
44. N. Takahashi *et al.*, TRPA1 underlies a sensing mechanism for O_2. *Nat. Chem. Biol.* **7**, 701–711 (2011).
45. J. P. Ward, Oxygen sensors in context. *Biochim. Biophys. Acta* **1777**, 1–14 (2008).
46. W. Cai *et al.*, Insulin regulates astrocyte gliotransmission and modulates behavior. *J. Clin. Invest.* **128**, 2914–2926 (2018).
47. L. M. Garcia-Segura, J. R. Rodriguez, I. Torres-Aleman, Localization of the insulin-like growth factor I receptor in the cerebellum and hypothalamus of adult rats: An electron microscopic study. *J. Neurocytol.* **26**, 479–490 (1997).
48. N. J. Abbott, L. Rönnbäck, E. Hansson, Astrocyte-endothelial interactions at the blood-brain barrier. *Nat. Rev. Neurosci.* **7**, 41–53 (2006).
49. T. M. Mathiisen, K. P. Lehre, N. C. Danbolt, O. P. Ottersen, The perivascular astroglial sheath provides a complete covering of the brain microvessels: An electron microscopic 3D reconstruction. *Glia* **58**, 1094–1103 (2010).
50. A. Agarwal *et al.*, Transient opening of the mitochondrial permeability transition pore induces microdomain calcium transients in astrocyte processes. *Neuron* **93**, 587–605.e7 (2017).
51. L. Beishon *et al.*, Vascular and haemodynamic issues of brain ageing. *Pflugers Arch.* **473**, 735–751 (2021).
52. A. Devor *et al.*, Stimulus-induced changes in blood flow and 2-deoxyglucose uptake dissociate in ipsilateral somatosensory cortex. *J. Neurosci.* **28**, 14347–14357 (2008).
53. N. Filippini *et al.*, Differential effects of the APOE genotype on brain function across the lifespan. *Neuroimage* **54**, 602–610 (2011).
54. N. Zhao *et al.*, Apolipoprotein E4 impairs neuronal insulin signaling by trapping insulin receptor in the endosomes. *Neuron* **96**, 115–129.e5 (2017).
55. A. Leuzy *et al.*, Longitudinal uncoupling of cerebral perfusion, glucose metabolism, and tau deposition in Alzheimer's disease. *Alzheimers Dement.* **14**, 652–663 (2018).
56. M. D. Devous, Sr, Functional brain imaging in the dementias: Role in early detection, differential diagnosis, and longitudinal studies. *Eur. J. Nucl. Med. Mol. Imaging* **29**, 1685–1696 (2002).
57. A. M. Fernandez, I. Torres-Alemán, The many faces of insulin-like peptide signalling in the brain. *Nat. Rev. Neurosci.* **13**, 225–239 (2012).
58. E. M. Rhea, C. Rask-Madsen, W. A. Banks, Insulin transport across the blood-brain barrier can occur independently of the insulin receptor. *J. Physiol.* **596**, 4753–4765 (2018).
59. R. U. Margolis, N. Altszuler, Insulin in the cerebrospinal fluid. *Nature* **215**, 1375–1376 (1967).
60. B. Pansky, J. S. Hatfield, Cerebral localization of insulin by immunofluorescence. *Am. J. Anat.* **153**, 459–467 (1978).
61. S. M. Gray, R. I. Meijer, E. J. Barrett, Insulin regulates brain function, but how does it get there? *Diabetes* **63**, 3992–3997 (2014).
62. T. Kuwabara *et al.*, Insulin biosynthesis in neuronal progenitors derived from adult hippocampus and the olfactory bulb. *EMBO Mol. Med.* **3**, 742–754 (2011).
63. M. W. Schwartz, D. Porte Jr., Diabetes, obesity, and the brain. *Science* **307**, 375–379 (2005).
64. W. A. Banks, J. B. Jaspan, W. Huang, A. J. Kastin, Transport of insulin across the blood-brain barrier: Saturability at euglycemic doses of insulin. *Peptides* **18**, 1423–1429 (1997).
65. M. Konishi *et al.*, Endothelial insulin receptors differentially control insulin signaling kinetics in peripheral tissues and brain of mice. *Proc. Natl. Acad. Sci. U.S.A.* **114**, E8478–E8487 (2017).
66. D. G. Baskin *et al.*, Quantitative autoradiographic evidence for insulin receptors in the choroid plexus of the rat brain. *Diabetes* **35**, 246–249 (1986).
67. H. J. Frank, W. M. Pardridge, W. L. Morris, R. G. Rosenfeld, T. B. Choi, Binding and internalization of insulin and insulin-like growth factors by isolated brain microvessels. *Diabetes* **35**, 654–661 (1986).
68. G. L. King, S. M. Johnson, Receptor-mediated transport of insulin across endothelial cells. *Science* **227**, 1583–1586 (1985).
69. A. Baron-Van Evercooren, C. Olichon-Berthe, A. Kowalski, G. Visciano, E. Van Obberghen, Expression of IGF-I and insulin receptor genes in the rat central nervous system: A developmental, regional, and cellular analysis. *J. Neurosci. Res.* **28**, 244–253 (1991).
70. M. Friesen, C. S. Hudak, C. R. Warren, F. Xia, C. A. Cowan, Adipocyte insulin receptor activity maintains adipose tissue mass and lifespan. *Biochem. Biophys. Res. Commun.* **476**, 487–492 (2016).
71. I. H. Manaserh *et al.*, Ablating astrocyte insulin receptors leads to delayed puberty and hypogonadism in mice. *PLoS Biol.* **17**, e3000189 (2019).
72. A. M. Fernandez *et al.*, Insulin regulates astrocytic glucose handling through cooperation with IGF-I. *Diabetes* **66**, 64–74 (2017).
73. A. M. Fernandez *et al.*, Regulation of the phosphatase calcineurin by insulin-like growth factor I unveils a key role of astrocytes in Alzheimer's pathology. *Mol. Psychiatry* **17**, 705–718 (2012).
74. L. Martinez-Rachadell *et al.*, Cell-specific expression of insulin/insulin-like growth factor-I receptor hybrids in the mouse brain. *Growth Horm. IGF Res.* **45**, 25–30 (2019).
75. A. M. Fernandez, S. Fernandez, P. Carrero, M. Garcia-Garcia, I. Torres-Aleman, Calcineurin in reactive astrocytes plays a key role in the interplay between proinflammatory and anti-inflammatory signals. *J. Neurosci.* **27**, 8745–8756 (2007).
76. A. Gomez-Arboledas *et al.*, Phagocytic clearance of presynaptic dystrophies by reactive astrocytes in Alzheimer's disease. *Glia* **66**, 637–653 (2018).
77. Y. Ma *et al.*, A three-dimensional digital atlas database of the adult C57BL/6J mouse brain by magnetic resonance microscopy. *Neuroscience* **135**, 1203–1215 (2005).
78. E. Hernandez-Garzón *et al.*, The insulin-like growth factor I receptor regulates glucose transport by astrocytes. *Glia* **64**, 1962–1971 (2016).
79. M. M. Behrens *et al.*, Ketamine-induced loss of phenotype of fast-spiking interneurons is mediated by NADPH-oxidase. *Science* **318**, 1645–1647 (2007).
80. D. Dávila, I. Torres-Aleman, Neuronal death by oxidative stress involves activation of FOXO3 through a two-arm pathway that activates stress kinases and attenuates insulin-like growth factor I signaling. *Mol. Biol. Cell* **19**, 2014–2025 (2008).